Semimetallic graphene in a modulated electric potential

J. H. Ho, Y. H. Chiu, S. J. Tsai, and M. F. Lin*
Department of Physics, National Cheng Kung University, Tainan 701, Taiwan
(Received 16 September 2008; revised manuscript received 16 January 2009; published 20 March 2009)

The π-electronic structure of graphene in the presence of a modulated electric potential is investigated by the tight-binding model. The low-energy electronic properties are strongly affected by the modulation period and potential strength. Such a potential could modify the energy dispersions, destroy state degeneracy, and induce band-edge states. One striking feature happens close to the Fermi level that the light-cone structure is replaced with two distinct kinds of valley structures with highly anisotropic energy dispersion. Both valleys are highlighted by the existence of the quasi-one-dimensional electronic states, whereas they are distinguished one from the other by the different directions of restricted motion of charge carriers. It should be noted that a modulated electric potential could make semiconducting graphene semimetallic, and that the onset period of such a transition relies on the field strength. The finite density of states (DOS) at the Fermi level means that there are free carriers, and, at the same time, the low DOS spectrum exhibits many prominent peaks, mainly owing to the band-edge states.

DOI: 10.1103/PhysRevB.79.115427 PACS number(s): 73.20.At, 73.22.−f, 81.05.Uw

I. INTRODUCTION

Carbon atoms could form diamond, graphites, carbon nanotubes, C60-related fullerenes, carbon onions, and carbon tori. These systems own special symmetric configurations, and their dimensionalities range from three dimensional (3D) to zero dimensional (0D). These systems are of great interest to community because of their spectacular physical properties to which the unique geometric structures give rise. Recently, a new carbon-based material is discovered by the success in experimental realization of fabricating a single graphene sheet,[1,2] and immediately this unique two-dimensional (2D) system becomes the focus of both theoretical and the experimental researches. One of the unique physical properties of the kind of system, for example, is the observation of an anomalous quantum Hall effect,[3] where the plateau of zero Hall conductance is unexpectedly absent. The novel phenomenon of Hall conductivity quantization is attributed to that the dynamics of quasiparticles in graphene is effectively relativistic, contrasting sharply with the conventional integer quantum Hall effect in the regular 2D electron system that is governed by the Schrödinger fermions.

Graphene has a honeycomb crystal structure with two distinct triangular sublattices A and B. This real-space structure corresponds to a triangular lattice in the reciprocal space, which also defines a hexagonal Brillouin zone with two inequivalent corners K and K'. The unique geometrical configuration of graphene leads to several nontrivial characteristics of its energy spectrum. There exist two identical low-energy bands in the vicinity of the two inequivalent corners, of which each exhibits a linear energy dispersion with conduction and valence bands crossing right at the corner. The highly diminished Fermi surface gives rise to a zero density of states (DOS) at the Fermi level, so graphene is a zero-gap semiconductor.

Studying the behavior of electrons under various kinds of external fields is not only of vital importance for understanding their physical nature of materials but also helpful for designing novel devices or developing applications. Many researches have been conducted on the physical properties of graphene, such as electronic properties,[4–6] transport properties,[1,7–10] optical properties,[11–13] and electronic excitations.[14–16] Here we focus on the effects of modulated fields on the electronic properties, an intriguing field of less exploration.[17–24] The systems for graphene in the modulated fields are not yet realized experimentally; however, the 2D free electron gas formed by GaAs/AlGaAs heterojunctions in modulated fields are well-established systems and have been subject of active studies in the past two decades.[25–28] For the 2D free electron gas, there are probably two types of periodic modulations in actual systems. One is an electrostatic modulation and the other is a magnetic-field modulation. The former can be realized by a periodic array of gate electrodes[26] and the latter by depositing magnetic materials on the surface.[27,28] In the case of magnetic modulation, the electronic properties of graphene have been recently studied.[21,23,24] In this paper, we would like to further investigate the electronic properties of graphene in a modulated electric potential. The tight-binding model is employed to calculate the energy spectrum and the density of states. Both are analyzed as functions of the field strength, the period, and the direction by solving the Hamiltonian matrix numerically. In this work, it is shown that semiconducting graphene can be made semimetallic by applying a modulated electric potential. Any finite value of field strength will cause such a transition with a prerequisite that the period of modulated potential is longer enough. However, a qualitative study, recently made by other authors, on the Dirac particles tunneling through a one-dimensional potential barrier predicts that the 2D light-cone structure is still preserved under such a field.[20] The underlying reason causing the different findings is elaborated in Sec. III.

This paper is organized as follows. The tight-binding Hamiltonian matrix in a periodic electric potential is derived in Sec. II. The main characteristics of the π-electronic structures are discussed in Sec. III. Finally, Sec. IV contains concluding remarks.

II. MODEL AND METHODS: TIGHT-BINDING MODEL

The π-electronic structure of graphene is calculated by the tight-binding model within the nearest-neighbor interactions. Given that graphene is a two-dimensional triangular lattice with two-point basis, we construct the π-electronic eigenfunction of the system as follows:

$$|\Psi_{\mathbf{k}}\rangle = C_{\mathbf{k}}^{A}|\Phi_{\mathbf{k}}^{A}\rangle + C_{\mathbf{k}}^{B}|\Phi_{\mathbf{k}}^{B}\rangle, \tag{1}$$

where the tight-binding Bloch function $|\Phi_{\mathbf{k}}^{A}\rangle$ ($|\Phi_{\mathbf{k}}^{B}\rangle$) is the superposition of the $2p_z$ orbitals from periodic A (B) atoms. The coefficients are obtained by diagonalizing the Hamiltonian matrix in the space spanned by the tight-binding Bloch functions. Moreover, with the two prerequisites that site energies for A and B atoms are the same, and that intrasublattice hoppings are ignored, we can set $\langle\Phi_{\mathbf{k}}^{A}|H_0|\Phi_{\mathbf{k}}^{A}\rangle = \langle\Phi_{\mathbf{k}}^{B}|H_0|\Phi_{\mathbf{k}}^{B}\rangle = 0$. The nonvanishing matrix elements are given by

$$\langle\Phi_{\mathbf{k}}^{B}|H_0|\Phi_{\mathbf{k}}^{A}\rangle = \frac{1}{N}\sum_{\mathbf{T}_i}\gamma_0 \exp\{-i\mathbf{k}\cdot\mathbf{T}_i\} \equiv \sum_i t_{i\mathbf{k}}, \quad i = 1,2,3, \tag{2}$$

where $\gamma_0 \equiv \int \varphi_{p_z}^{*}(\mathbf{r}-\mathbf{R}_A)H_0\varphi_{p_z}(\mathbf{r}-\mathbf{R}_A-\mathbf{T}_i)d^3r \simeq 2.6$ eV is the nearest-neighbor hopping integral with R_A being the lattice vector and φ_{p_z} being the atomic $2p_z$ orbital. $\mathbf{T}_i$ are the vectors connecting a carbon atom to its three nearest neighbors, and they are given by $\mathbf{T}_1 = (b/2, \sqrt{3}b/2)$, $\mathbf{T}_2 = (b/2, -\sqrt{3}b/2)$, and $\mathbf{T}_3 = (-b, 0)$, where $b = 1.42$ Å is the C-C bond length. $t_{i\mathbf{k}}$, denoting individual hopping process, is then explicitly given by $t_{1\mathbf{k}} = \gamma_0 \exp[(ik_x b/2 + ik_y\sqrt{3}b/2)]$, $t_{2\mathbf{k}} = \gamma_0 \exp[(ik_x b/2 - ik_y\sqrt{3}b/2)]$, and $t_{3\mathbf{k}} = \gamma_0 \exp(-ik_x b)$. After specifying the matrix elements, the zero-field Hamiltonian is expressed as the following 2×2 Hermitian matrix:

$$\begin{pmatrix} 0 & \sum_i t_{i\mathbf{k}}^{*} \\ \sum_i t_{i\mathbf{k}} & 0 \end{pmatrix}. \tag{3}$$

The Hamiltonian matrix can be solved analytically and it generates two energy dispersions represented by $E_{\pm}(\mathbf{k}) = \pm\gamma_0[1 + 4\cos^2(\sqrt{3}k_y b/2) + 4\cos(\sqrt{3}k_y b/2)\cos(3bk_x/2)]^{1/2}$. The low-energy spectrum shows symmetry between two valleys (around K and K'), where both have the identical light-cone structure described by the relation $E_{\pm}(\mathbf{q}) = \pm v_F|\mathbf{q}|$, with light velocity $v_F \equiv 3b\gamma_0/2$ and momentum $\mathbf{q}$ measuring the difference $\mathbf{q} = \mathbf{k} - \mathbf{k}_K$ ($\mathbf{k} - \mathbf{k}_{K'}$) in wave vector $\mathbf{k}$ and corner $\mathbf{k}_K$ ($\mathbf{k}_{K'}$) of the Brillouin zone.

Consider graphene that exists in a 1D modulated potential $U(x)$ along the armchair direction ($\hat{x}$) and the potential profile is assumed to take the form $U(x) = V_0\cos(2\pi x/l_E)$ with V_0 being the field strength. For convenience, the period l_E is further designed to be a multiple of $3b$, with $l_E = 3bR_E$. In doing so, the periodicity caused by such a field is made commensurate with the crystal potential of graphene itself, which helps define a primitive cell. The rectangular primitive cell is enlarged to include $4R_E$ carbon atoms denoted as A_n (B_n) with $n = 1,2,\ldots,2R_E$ for A- (B-) type carbon atoms [Fig. 1(a)]. The corresponding rectangular Brillouin zone shrinks to be $1/2R_E$ of the original hexagonal Brillouin zone and its dimension along the modulated direction ($|k_x| \leq \pi/3bR_E$) is relatively shorter than the other one ($|k_y| \leq \pi/\sqrt{3}b$), as shown in Fig. 1(b). The eigenfunction of a system is the superposition of elements in the basis composed of $4R_E$ Bloch functions,

$$\{|\phi_{\mathbf{k}}^{A_1}\rangle, |\phi_{\mathbf{k}}^{B_1}\rangle, |\phi_{\mathbf{k}}^{A_2}\rangle, |\phi_{\mathbf{k}}^{B_2}\rangle, \ldots |\phi_{\mathbf{k}}^{A_{2R_E-1}}\rangle, |\phi_{\mathbf{k}}^{B_{2R_E-1}}\rangle, |\phi_{\mathbf{k}}^{A_{2R_E}}\rangle, |\phi_{\mathbf{k}}^{B_{2R_E}}\rangle\},$$

and is represented as

$$|\Psi_{\mathbf{k}}\rangle = \sum C_{\mathbf{k}}^{A_n}|\Phi_{\mathbf{k}}^{A_n}\rangle + C_{\mathbf{k}}^{B_n}|\Phi_{\mathbf{k}}^{B_n}\rangle. \tag{4}$$

When the period is sufficiently large, the effects of the electric potential on the off-diagonal matrix elements are negligible. Meanwhile, the diagonal matrix elements would become

$$\langle\Phi_{\mathbf{k}}^{A_n}|H|\Phi_{\mathbf{k}}^{A_n}\rangle = V_0\cos[(n-1)\pi/R_E] \equiv U_n,$$

$$\langle\Phi_{\mathbf{k}}^{B_n}|H|\Phi_{\mathbf{k}}^{B_n}\rangle = V_0\cos[(n-2/3)\pi/R_E] \equiv U_{n+1/3}, \tag{5}$$

where $H = H_0 + U$ is the total Hamiltonian. In effect, the assumption made above is plausible. The period (≥ 0.1 μm) in a typical experimental setup is still much longer than the

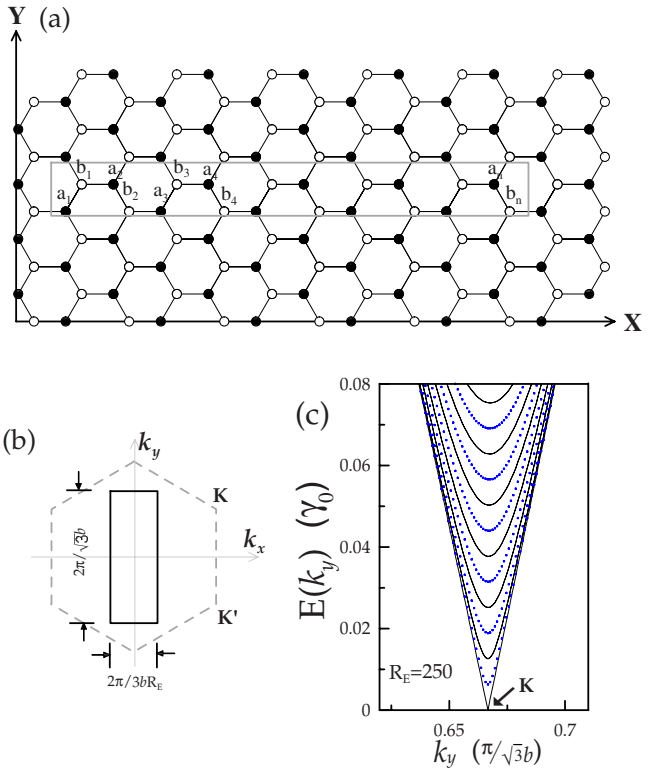

FIG. 1. (Color online) (a) The rectangular primitive cell of graphene in a modulated electric potential along the armchair direction ($\hat{x}$). The rectangular first Brillouin zone is shown in (b), and the hexagon is that without external fields. The k_y-dependent low-energy bands without any fields at $R_E = 250$ is shown in (c) for $k_x = 0$ (black solid lines) and $k_x = 2\pi/3bR_E$ (blue dotted lines).

extension of atomic $2p_z$ orbital (≈ 1 Å), so the atomic orbital feels approximately a constant potential within its distribution. To facilitate the calculation, the basis functions are further rearranged in a specific sequence to obtain the band Hamiltonian matrix

$$\{|\phi_{\mathbf{k}}^{A_1}\rangle, |\phi_{\mathbf{k}}^{B_{2R_E}}\rangle, |\phi_{\mathbf{k}}^{B_1}\rangle, |\phi_{\mathbf{k}}^{A_{2R_E}}\rangle, \ldots |\phi_{\mathbf{k}}^{A_{R_E}}\rangle, |\phi_{\mathbf{k}}^{B_{R_E+1}}\rangle, |\phi_{\mathbf{k}}^{B_{R_E}}\rangle, |\phi_{\mathbf{k}}^{A_{R_E+1}}\rangle\}.$$

The band Hamiltonian matrix of graphene in a modulated electric potential along the armchair direction is written as

$$\begin{pmatrix} U_1 & q & p^* & 0 & \cdots & \cdots & 0 & 0 \\ q^* & U_{2R_E+1/3} & 0 & p & 0 & \cdots & \cdots & 0 \\ p & 0 & U_{4/3} & 0 & q^* & 0 & \cdots & 0 \\ 0 & p^* & 0 & U_{2R_E} & 0 & q & 0 & 0 \\ \vdots & \ddots & q & 0 & U_2 & \ddots & \ddots & 0 \\ \vdots & \cdots & \ddots & q^* & \ddots & \ddots & 0 & p \\ 0 & \vdots & \vdots & \ddots & \ddots & 0 & U_{R_E+1/3} & q^* \\ 0 & 0 & 0 & 0 & 0 & p^* & q & U_{R_E+1} \end{pmatrix} \tag{6}$$

with $p \equiv t_{1\mathbf{k}} + t_{2\mathbf{k}}$ and $q \equiv t_{3\mathbf{k}}$.

Graphene owns the anisotropic geometry, so that the π-electronic structure could depend on the modulation direction. When the modulation direction is changed into the zigzag direction ($\hat{x}$), the diagonal matrix element becomes

$$\langle \Phi_{\mathbf{k}}^{A_n} | H | \Phi_{\mathbf{k}}^{A_n} \rangle = \langle \Phi_{\mathbf{k}}^{B_n} | H | \Phi_{\mathbf{k}}^{B_n} \rangle = U_n. \tag{7}$$

In this case, the period is designed as $l_E' = \sqrt{3} b R_E$ for the same reason mentioned earlier in the armchair case. The corresponding rectangular Brillouin zone also shrinks to be $1/2R_E$ of the original hexagonal Brillouin zone and its dimension is characterized by $|k_x| \leq \pi/\sqrt{3} b R_E$ along the zigzag direction and $|k_y| \leq \pi/3b$ along the other. The Hamiltonian matrix can be easily constructed in a similar way to that in the armchair case (not shown here).

In the following discussion, we will consider the situation that the actual modulation period is about submicron length, which corresponds to $R_E \approx 250$. This involves a process of diagonalizing a very large Hamiltonian matrix, and it is solved numerically to obtain the energy bands. Due to the resulting unoccupied conduction bands (E^c) and occupied valence bands (E^v) symmetric about the Fermi level ($E_F = 0$), we only discuss the former.

III. ELECTRONIC PROPERTIES

Before presenting the results under a modulated electric potential, a brief review of the main features of low-energy bands of the zero-potential system is made. As mentioned earlier, the low-energy band structure has a linear energy dispersion around K or K' of the hexagon. However, it is not convenient to compare directly with the coming case when a modulated potential is present because they are presented in different Brillouin zones. To treat them on an equal footing, the unit cell of the zero-field system is chosen to be identical to the primitive cell of the system in a modulated potential. That is, if the modulated field has a period R_E, the unit cell is chosen to be $2R_E$ times its primitive cell. In this way, all electronic states in the hexagonal Brillouin zone are folded into a rectangular one. Notice that such a folding method guarantees not to change any features of the original band structure. Figure 1(c) shows the k_y dependence of the low-energy spectrum at $R_E = 250$ for $k_x = 0$ (black solid lines) and $k_x = \pi/3bR_E$ (blue dotted lines). There exists a nondegenerate 1D linear band and doubly degenerate 1D parabolic bands for $k_x = 0$, while they are purely doubly degenerate 1D parabolic bands for $k_x = \pi/3bR_E$. The evolution of bands from $k_x = 0$ to $k_x = \pi/3bR_E$ fills the states between them, which reflects the 2D characteristic of the light-cone structure. (This energy spectrum corresponds to one of the two valleys containing the Dirac point K now located at $k_x = 0$ and $k_y = 2\pi/3\sqrt{3}b$.) Above the Dirac point, there exists a local minima for each 1D parabolic band. Notice that these points should not be considered as band-edge states. For these states, the k_x-dependent energy dispersion is linear with nonzero first derivative, so they cannot be treated as critical points in the energy-momentum space. The band structure is in all respects the same as one before folding the zone. Although this alternative representation of band structure somewhat complicates the explanation, it is advantageous for the following discussion to compare the zero-potential system and the system in a modulated electric potential.

A modulated electric potential has a strong effect on the energy dispersions, state degeneracy, and band-edge states. The k_y-dependent conduction bands for $k_x = 0$ (black solid lines) and $k_x = \pi/3bR_E$ (blue dotted lines) are shown in Fig. 2(a) for the modulated electric potential along the armchair direction with the period $R_E = 250$ (≈ 100 nm) and the strength $V_0 = 0.025\gamma_0$. Moreover, the potential mainly affects the structure of some low 1D bands. The original doubly degenerate parabolic bands are split. The energy dispersions around $k_y = 2\pi/3\sqrt{3}b \equiv k_y^K$ are strongly deformed and induce several band-edge states which are saddle points in the energy-momentum space. These band-edge states always appear in pairs at two sides of k_y^K and two band-edge states in each pair might have small energy difference. Far away from k_y^K, the spectrum is almost linear for the k_y dependence, while it becomes dispersionless for the k_x dependence, which can been seen in Fig. 2(a) where the bands for $k_x = 0$ and $k_x = \pi/3bR_E$ have identical dispersion. It is important to note that there exist more Fermi momentum states k_F's. The energy dispersions near k_F's are linear for the k_y dependence, while they are completely flat for the k_x dependence. The dispersionless feature means that the number of the Fermi-momentum states is infinite, which sharply contrasts with the original two Fermi-momentum states or Dirac points in zero-field graphene. Besides, the nonzero measure of the Fermi surface indicates finite value of the DOS at the Fermi level.

The aforementioned features might rely on the strength, period, and direction of a modulated electric potential. The modulation effects are even enhanced when potential is strengthened, as illustrated in the Fig. 2(b). When the strength increases, more low 1D bands are affected. The energy bands are further deformed and more band-edge states are created. In addition, the number of Fermi-momentum states increases almost linearly with the potential strength.

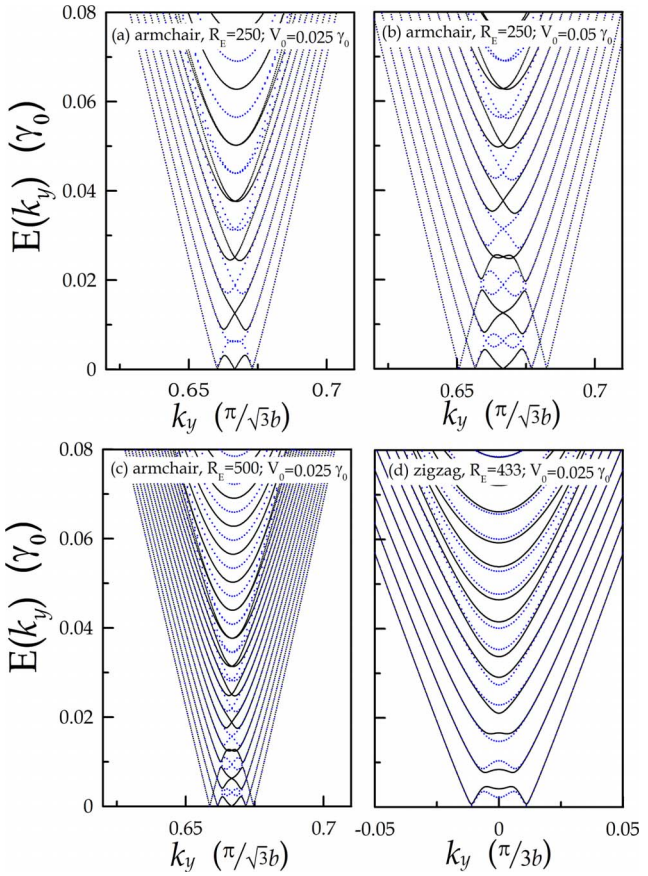

FIG. 2. (Color online) The k_y-dependent low-energy bands in the modulated potential along armchair direction with $V_0=0.025\gamma_0$ and $R_E=250$ for $k_x=0$ (black solid lines) and $k_x=2\pi/3bR_E$ (blue dotted lines) those in a stronger potential with $V_0=0.05\gamma_0$ and those in the potential of a longer period $R_E=500$ are, respectively, shown in (a), (b), and (c). (d) is the k_y dependence of low-energy bands at $V_0=0.025\gamma_0$ and $R_E=433$ with the potential modulating along the zigzag direction for $k_x=0$ (black solid lines) and $k_x=2\pi/\sqrt{3}bR_E$ (blue dotted lines). Notice that the actual periods in (a) and (d) are almost of equal length, and that the units of k_y are different for armchair $(\pi/\sqrt{3}b)$ and zigzag $(\pi/3b)$ directions.

For the case in Fig. 2(b), the number of Fermi-momentum states is approximately double of that in Fig. 2(a). The modulation period can also affect the numbers of band-edge states and Fermi-momentum states, as shown in Fig. 2(c). When the period increases, more band-edge states are created. The number of Fermi-momentum states remains almost unchanged in the long-period regime, whereas there is a drastic change in the short-period regime. The former can be understood by taking into consideration both the accompanying reduced k_x length and increased k_F's associated with different k_y's in accordance with the increasing period, while the latter will be discussed later by calculating the density of states at the Fermi level. The low-energy bands are, on the other hand, not sensitive to the direction of a modulated electric potential. Figure 2(d), for example, presents the bands for the potential modulated along the zigzag direction.

A closer examination of energy states around the Fermi level reveals the highly anisotropic properties of quasiparticles. For that, we present the contour plots around the Fermi

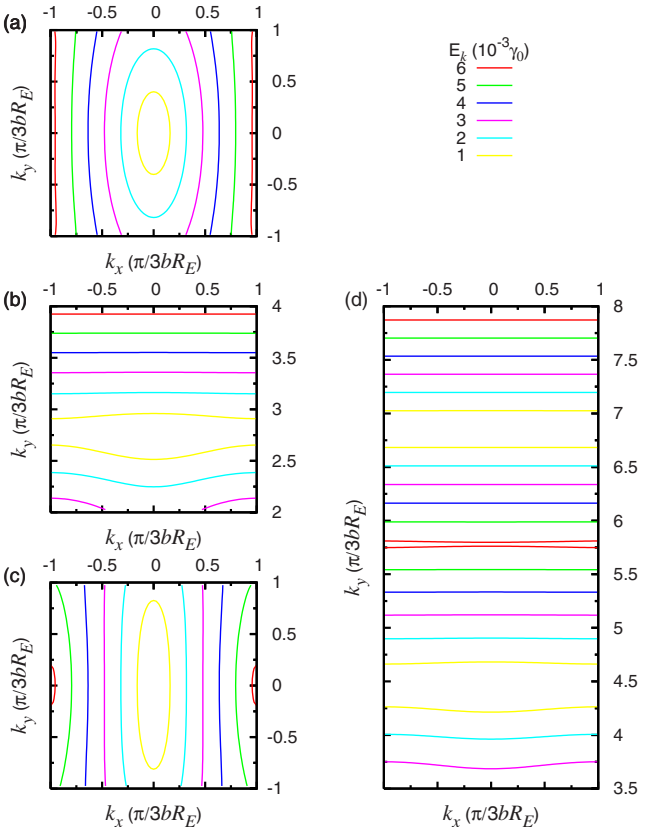

FIG. 3. (Color online) The contour plot of the first conduction band around the Fermi level for the considered modulated electric potentials with $V_0=0.025\gamma_0$ and $R_E=250$ in (a) and (b) and $V_0=0.05\gamma_0$ and $R_E=250$ in (c) and (d). The energy difference between neighboring contours is $1.0\times10^{-3}\gamma_0$. For clarity, the origin of coordinate k_y is shifted to $k_y=k_y^K$.

level of the lowest conduction band in Figs. 3(a)–3(d), in which Figs. 3(a) and 3(b) [Figs. 3(c) and 3(d)] are the energy contours corresponding to the lowest conduction band of Fig. 2(a) [Fig. 2(b)]. The energy dispersion around the Dirac point [Fig. 3(a)] shows that the group velocity of quasiparticles is strongly renormalized perpendicular to the modulation direction whereas it is not renormalized at all parallel to the modulation direction. As the potential strength is raised, the group velocity along the y direction is further reduced, and approaches zero, as shown in Fig. 3(c). This unique behavior is attributed to the chirality of charge carriers, which was also reported by Park *et al.*[29,30] recently. On the other hand, there are other band crossings [Figs. 3(b) and 3(d)] occurring at the Fermi level far away from the Dirac point. Very differently, the quasiparticles here dramatically change their character in such a way that the energy dispersion is almost linear along the k_y direction and dispersionless along the other. In general, the two above-mentioned kinds of distinct valley structures associated with states near the Fermi level are of equal importance in studying essential physical properties. However, as we have indicated in the paper, the finite DOS at the Fermi level is mainly due to the states coming from the valleys far away from the Dirac point. This implies that they form the majority of charge carriers as the potential strength is increased and thus dominate the essential physical properties.

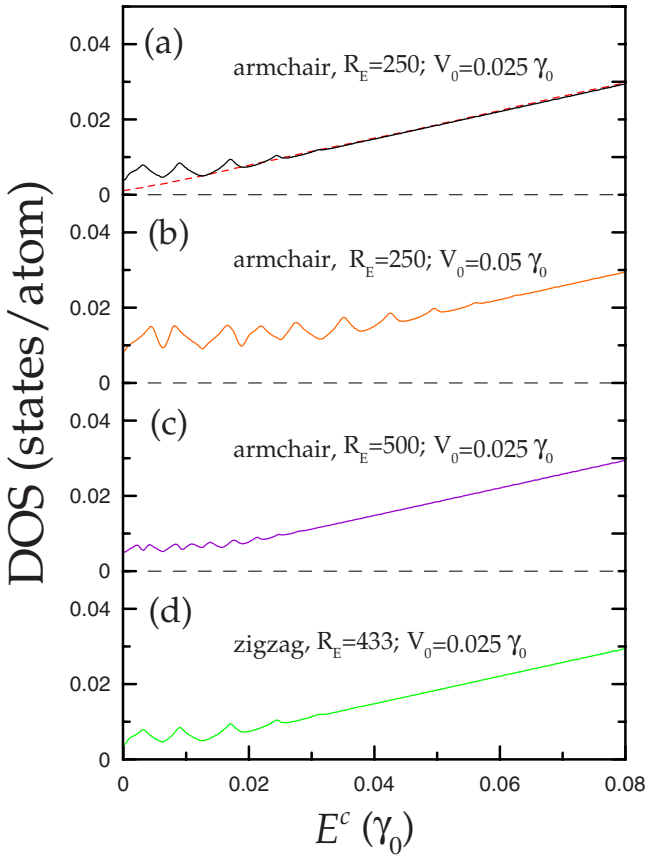

FIG. 4. (Color online) The low-frequency density of states for the potential modulated along armchair direction at (a) $V_0=0.025\gamma_0$ and $R_E=250$, (b) $V_0=0.05\gamma_0$ and $R_E=250$, (c) $V_0=0.025\gamma_0$ and $R_E=500$, and (d) along the zigzag direction at $V_0=0.025\gamma_0$ and $R_E=433$. The dashed line in (a) is for the zero-potential spectrum.

The essential features of electronic structure are directly reflected on the density of states and defined as

$$D(\omega)=\sum_{\sigma,h=c,v}\int_{1\text{st BZ}}\frac{dk_x dk_y}{(2\pi)^2}\frac{\Gamma}{\pi}\frac{1}{[\omega-E^h(k_x,k_y)]^2+\Gamma^2}. \quad (8)$$

Γ ($=5\times10^{-5}\gamma_0$) is the phenomenological broadening parameter. Because of the linear energy dispersion, the low-frequency DOS without potentials is proportional to ω, as shown by dotted line in Fig. 4(a), and it has no special structures. The vanishing DOS at $E_F=0$ indicates that graphene is a zero-gap semiconductor. A modulated electric potential can lead to many prominent peaks and a finite DOS at $\omega=0$ [Figs. 4(a)–4(d)]. The peak structures come from the band-edge states of parabolic bands [Figs. 2(a)–2(d)]. The frequency, number, and height of peaks are sensitive to the changes in the potential strength and period. The DOS at the Fermi level means that there are free carriers, so graphene becomes a semimetal in the presence of a modulated electric potential. The value of DOS at $\omega=0$ grows as the potential strength increases [Figs. 4(a) and 4(b)]. However, it does not change significantly as the period is varied [Fig. 4(c)]. Moreover, the low-frequency DOS is unaltered when the modulation direction changes [Fig. 4(d)], which reflects the isotropic symmetry of graphene in the low-energy spectrum.

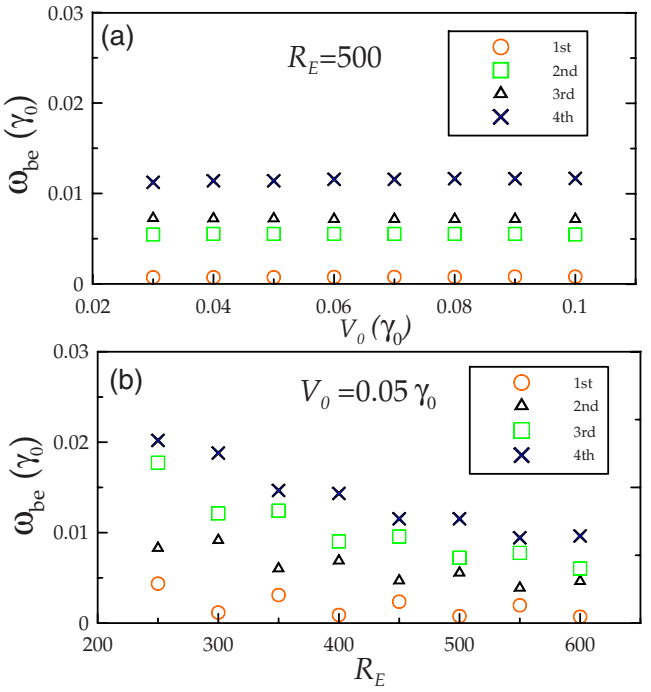

FIG. 5. (Color online) Energies of the first four prominent peaks versus (a) the potential strength at $R_E=500$ and (b) the modulation period at $V_0=0.05\gamma_0$.

The singularities in the DOS might cause special structures in some physical quantities, for example, giving rise to the strong absorption peaks in optical measurements, so it is worthy to investigate their properties in detail. The peak height, number, and frequency are dominated by the strength and period of the potential [Figs. 4(a)–4(c)]. The peak height is enhanced by the increasing strength, whereas it is reduced by the increasing period. The peak number is increased by both the increasing strength and period. The relations between the peak frequency (ω_{be}) and the field condition are elaborated through examining the first four prominent peaks, as shown in the Fig. 5(a) for the strength dependence and Fig. 5(b) for the period dependence. From these, it is observed that the peak frequency weakly depends on the strength, while it declines gradually and presents somewhat oscillatory behavior as the period increases.

The nonzero DOS at the Fermi level, in connection with the degree of band overlap between conduction and valence bands, serves as an indicator of the semimetallic transition. Here, we examine the relationship between the DOS at $\omega=0$ and the potential strength, and that between the DOS at $\omega=0$ and the modulation period. Referring to Fig. 6(a), $D(\omega=0)$ shows a nearly linear variation with the potential strength. This relation just reflects the fact that the number of Fermi-momentum states is approximately proportional to potential strength. On the other hand, the period dependence of $D(\omega=0)$ exhibits different features in short- and long-period regimes, as shown in Fig. 6(b). The two regimes are distinguished by a threshold period R_{th}, which happens at $R_E\approx100$ for $V_0=0.025\gamma_0$ [black triangles in Fig. 6(b)] and becomes shorter as the potential strength gets stronger [red

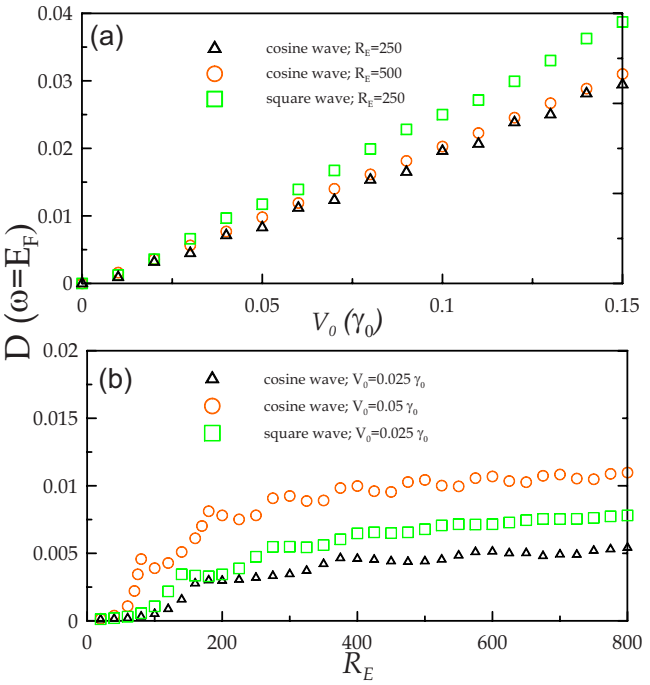

FIG. 6. (Color online) The density of states at the Fermi level versus (a) the potential strength at R_E=250 and 500 (R_E=250) for the modulated potential of cosine-wave (square-wave) profile and versus (b) the modulation period at V_0=0.025γ_0 and 0.05γ_0 (V_0 =0.025γ_0) for that of the cosine-wave (square-wave) profile.

circles in Fig. 6(b)]. For $R_E \ll R_{\text{th}}$, $D(\omega=0)$ remains zero as R_E increases from zero, which implies that the 2D light-cone structure is not affected at such a short period. As R_E is increased to cross R_{th}, $D(\omega=0)$ quickly grows and saturates to a definite value, with some fluctuations in the long-period regime. If one considers a realistic experimental system, the typical modulation period will be about submicron or even longer. $D(\omega=0)$ then would fall into the long-period regime, so its value does not change significantly as the period is somewhat varied. In other words, this feature should be very robust even there exist some inevitable period fluctuations coming from processing devices or experimental setups.

These interesting features, including potential-induced band-edge states and the semimetallic behavior of graphene, caused by a modulated electric potential are the main results in this work. Nevertheless, the semimetallic behavior, the most important feature, was not obtained in a recent study.[20] The study considered graphene subjected to a square-wavelike modulated potential, concluding that the 2D light-cone structure is still preserved. Although the conclusion seems to contradict with our results given here, a in-depth examination shows that this is not the case. The main discrepancy lies in the fact that the modulation period used (20 nm$\approx R_E$=50) in their calculation is too short to achieve the threshold (R_{th}), so that the semimetallic behavior was not observed. To clarify this point, the dependence of $D(\omega=0)$ on the potential strength and the modulation period for a square-wave potential is calculated here, as shown by green squares in Figs. 6(a) and 6(b), respectively. $D(\omega=0)$ in Fig. 6(a) exhibits a linear relation with the potential strength, which is similar to the cosine-wave potential. The threshold period in this case is $R_{\text{th}} \approx 100$ [Fig. 6(b)], which is close to that in the cosine-wave potential. As a result, from Fig. 6(b), it self-evidently explains the reason why the semimetallic behavior is not observed by other authors solely because that R_E taken in their calculation is less than R_{th}.

IV. CONCLUDING REMARKS

In summary, the tight-binding model is used to investigate the effects of a modulated electric potential on the π-electronic structure of graphene. The low-energy electronic properties are mainly dominated by the potential strength and period. However, they are not sensitive to the potential direction, which is due to the isotropy of the original low-energy bands. A modulated electric potential drastically changes the energy dispersions, state degeneracy, and band-edge states. Close to the Fermi level, the light-cone structure is replaced with two distinct kinds of valley structures with highly anisotropic energy dispersions. Both kinds of valley structures can exhibit dispersionless feature in one direction, with one kind being perpendicular to the modulation direction whereas the other being parallel to it. Notice that the dispersionless feature gives rise to infinite Fermi-momentum states. The density of states exhibits a lot of prominent peaks. These structures are mainly determined by the energy dispersions and the band-edge states. The finite DOS at the Fermi level indicates the existence of free carriers. The semiconducting graphene becomes semimetallic by applying a modulated electric potential, as long as the period surpasses a threshold period ($R_E \gg R_{\text{th}}$). Different nature of the low-energy excitations for graphene in the presence of a modulated potential is expected to give rise intriguing physical properties. For instance, the free electrons are expected to cause the low-frequency plasmon. The theoretical predictions could be tested by the experimental measurements on the energy loss spectra.

ACKNOWLEDGMENTS

This work was supported by NSC and NCTS of Taiwan under Grant No. NSC 96-2112-M-006-002.

*mflin@mail.ncku.edu.tw

[1] K. S. Novoselov, A. K. Geim, S. V. Morozov, D. Jiang, Y. Zhang, S. V. Dubonos, I. V. Grigorieva, and A. A. Firsov, Science **306**, 666 (2004).

[2] C. Berger *et al.*, J. Phys. Chem. B **108**, 19912 (2004).

[3] K. S. Novoselov, A. K. Geim, S. V. Morozov, D. Jiang, M. I. Katsnelson, I. V. Grigorieva, S. V. Dubonos, and A. A. Firsov, Nature (London) **438**, 197 (2005).

[4] A. Bostwick, T. Ohta, T. Seyller, K. Horn, and E. Rotenberg, Nat. Phys. **3**, 36 (2007).
[5] N. M. R. Peres, F. Guinea, and A. H. Castro Neto, Phys. Rev. B **73**, 125411 (2006).
[6] B. Partoens and F. M. Peeters, Phys. Rev. B **75**, 193402 (2007).
[7] V. P. Gusynin and S. G. Sharapov, Phys. Rev. Lett. **95**, 146801 (2005).
[8] S. Adam, E. H. Hwang, V. M. Galitski, and S. Das Sarma, Proc. Natl. Acad. Sci. U.S.A. **104**, 18392 (2007).
[9] Z. Jiang, Y. Zhang, H. L. Stormer, and P. Kim, Phys. Rev. Lett. **99**, 106802 (2007).
[10] K. S. Novoselov, Z. Jiang, Y. Zhang, S. V. Morozov, H. L. Stormer, U. Zeitler, J. C. Maan, G. S. Boebinger, P. Kim, and A. K. Geim, Science **315**, 1379 (2007).
[11] M. L. Sadowski, G. Martinez, M. Potemski, C. Berger, and W. A. de Heer, Phys. Rev. Lett. **97**, 266405 (2006).
[12] M. L. Sadowski, G. Martinez, M. Potemski, C. Berger, and W. A. de Heer, Solid State Commun. **143**, 123 (2007).
[13] V. P. Gusynin, S. G. Sharapov, and J. P. Carbotte, Phys. Rev. Lett. **98**, 157402 (2007).
[14] F. Guinea, Phys. Rev. B **75**, 235433 (2007).
[15] E. H. Hwang and S. Das Sarma, Phys. Rev. B **75**, 205418 (2007).
[16] X.-F. Wang and T. Chakraborty, Phys. Rev. B **75**, 033408 (2007).
[17] A. Matulis and F. M. Peeters, Phys. Rev. B **75**, 125429 (2007).
[18] M. Tahir and K. Sabeeh, Phys. Rev. B **76**, 195416 (2007).
[19] M. Tahir and K. Sabeeh, Phys. Rev. B **77**, 195421 (2008).
[20] M. Barbier, F. M. Peeters, P. Vasilopoulos, and J. J. M. Pereira, Phys. Rev. B **77**, 115446 (2008).
[21] M. Ramezani Masir, P. Vasilopoulos, A. Matulis, and F. M. Peeters, Phys. Rev. B **77**, 235443 (2008).
[22] S. Park and H. S. Sim, Phys. Rev. B **77**, 075433 (2008).
[23] Y. H. Chiu, Y. H. Lai, J. H. Ho, D. S. Chuu, and M. F. Lin, Phys. Rev. B **77**, 045407 (2008).
[24] J. H. Ho, Y. H. Lai, Y. H. Chiu, and M. F. Lin, Nanotechnology **19**, 035712 (2008).
[25] R. R. Gerhardts, D. Weiss, and K. v. Klitzing, Phys. Rev. Lett. **62**, 1173 (1989).
[26] A. Messica, A. Soibel, U. Meirav, A. Stern, H. Shtrikman, V. Umansky, and D. Mahalu, Phys. Rev. Lett. **78**, 705 (1997).
[27] M. Kato, A. Endo, S. Katsumoto, and Y. Iye, Phys. Rev. B **58**, 4876 (1998).
[28] M. Kato, A. Endo, M. Sakairi, S. Katsumoto, and Y. Iye, J. Phys. Soc. Jpn. **68**, 1492 (1999).
[29] C.-H. Park, L. Yang, Y.-W. Son, M. L. Cohen, and S. G. Louie, Nat. Phys. **4**, 213 (2008).
[30] C.-H. Park, Y.-W. Son, L. Yang, M. L. Cohen, and S. G. Louie, Nano Lett. **8**, 2920 (2008).